Journal of Catalysis 273 (2010) 199–210

Contents lists available at ScienceDirect

Journal of Catalysis

journal homepage: www.elsevier.com/locate/jcat

Photocatalytic oxidation of cyclohexane by titanium dioxide: Catalyst deactivation and regeneration

Joana T. Carneiro [a], Jacob A. Moulijn [a], Guido Mul [b,*]

[a] Catalysis Engineering, DelftChemTech, Delft University of Technology, Julianalaan 136, 2628 BL Delft, The Netherlands
[b] PhotoCatalytic Synthesis Group, IMPACT Institute, Faculty of Science and Technology, University of Twente, P.O. Box 217, 7500 AE Enschede, The Netherlands

ARTICLE INFO

Article history:
Received 25 February 2010
Revised 4 May 2010
Accepted 22 May 2010
Available online 1 July 2010

Keywords:
TiO_2
Deactivation
Regeneration
Crystallinity
Particle size
ATR
Stability
Photoreactor
Photocatalysis
Selective oxidation

ABSTRACT

Two commercially available TiO_2 catalysts were compared in the selective photocatalytic oxidation of cyclohexane: Hombikat UV100 (as received (H), and after calcination at 600 °C (H600)), and Solaronix, S450. Hombikat UV100 shows the highest initial activity on a g^{-1} catalyst basis, followed by H600 and S450 with very similar activity profiles. All catalysts suffer from deactivation. By *in situ* ATR and DRIFT spectroscopy, it is demonstrated that the extent, nature, and thermal stability of carboxylates and carbonates formed on the surface of the three catalysts are quite different. The extent of carboxylate formation was significantly smaller on the surfaces of H600 and S450, when compared to H. The thermal stability of the surface species at 400 °C decreased in the order H > H600 > S450. Complete removal of carboxylate and carbonate species from the surface was only achieved in the case of S450, which resulted in complete regeneration of activity, as demonstrated in both a slurry reactor (top illumination reactor) and internally illuminated monolith reactor (IIMR). The differences in surface chemistry and regenerability are discussed on the basis of lattice defects, affecting the opto-electronic properties, and defects/irregularities on the surface, affecting (thermal) stability of surface-adsorbed species. Solaronix S450 is the preferred catalyst for the desired conversion, the favorable surface properties being an important first step toward the practical application of photocatalysis in selective liquid-phase photo-oxidation processes and in particular toward employment of reactors with immobilized TiO_2 in the photocatalytic oxidation of cyclohexane.

1. Introduction

Photocatalysis applying semiconductor materials has attracted many researchers active in the disciplines of physical chemistry, material science, catalysis, and reactor engineering. By far the most research activity in photocatalysis is in the field of environmental pollution abatement, such as air cleaning and wastewater purification, in which organic compounds are totally oxidized into carbon dioxide and water over mainly TiO_2-based photocatalysts [1–3]. Photocatalytic synthetic processes using selective oxidation have been less well developed. Nevertheless, several studies show that high selectivities can be achieved in TiO_2 catalyzed photo-oxidation, when compared to conventional oxidation processes [4,5]. Selective photocatalytic oxidation of cyclohexane in the liquid phase to cyclohexanone and cyclohexanol is of particular interest. This is an important commercial reaction since cyclohexanone is the caprolactam precursor, a monomer for nylon-6 production. High ketone selectivities were reported by several authors [6–12]. Several parameters for optimization of the photocatalytic process have been considered, such as the type of photoreactor [8,13,14], catalyst modification [9,12,15], and choice of solvent [6,7,16]. More recently by the usage of operando techniques [17], novel insight into the mechanism of this reaction, and the pathways leading to catalyst deactivation were reported. Strongly adsorbed intermediates and products (cyclohexanone) are further oxidized to carboxylates and carbonates, which quickly deactivate the catalyst [17].

Currently photoreactors for liquid-phase oxidation are typically based on slurry systems, *i.e.*, the catalyst particles are dispersed within the liquid in the reactor. Although this design offers ease of construction and high catalyst loading, it has clearly drawbacks, such as the difficulty of separation of catalyst particles from the reaction mixture and low light utilization efficiencies due to the scattering and shielding of light by the reaction medium and catalyst particles. Recently, an internally illuminated monolith reactor was developed where the light is distributed through side light optical fibers in monolith channels, which contain the catalyst [14]. This design, with the fibers tip-coated with a reflective material and the catalyst coated on the walls of the monolith, decouples the light propagation process in the fiber from the physical properties of the catalytic layer, which positively affects the photonic efficiency [14,18]. Furthermore, such reactor opens the possibility for

* Corresponding author. Fax: +31 53 4892882.
E-mail addresses: g.mul@utwente.nl, g.mul@tudelft.nl (G. Mul).

0021-9517/$ - see front matter © 2010 Elsevier Inc. All rights reserved.
doi:10.1016/j.jcat.2010.05.015

a continuous process. For this to become feasible in practice, the catalyst coating used needs to be optimized, limiting catalyst deactivation, or at least allowing complete regeneration of activity in a rejuvenation process step.

In the present study, we demonstrate by comparing three TiO_2 catalysts that crystallinity and surface structure have an important influence on (i) the desorption rate of cyclohexanone, (ii) the surface chemistry leading to carboxylates and carbonates, and (iii) the thermal stability of these deactivating species. The preferred Solaronix S450 TiO_2 shows favorable product desorption, as well as low thermal stability of the adsorbed species formed during reaction, and is the preferred material for practical application, as demonstrated in the application of the internally illuminated monolith reactor (IIMR).

2. Materials characterization and testing

2.1. Materials and characterization

In this work, two commercially available TiO_2 materials were compared: the 100% pure anatase Hombikat UV100 from Sachtleben™ (H) and a TiO_2 paste, Ti nanoxide from Solaronix™, used for solar cell applications [19]. The Solaronix nanopowder is provided in a colloidal suspension (11 wt%) in butanol prepared by wet precipitation with a nominal particle size of 10 nm [19]. This material is specifically designed for coatings (immobilized systems) and was obtained in the final form by calcination in static air for 15 min at 450 °C, applying a heating rate of 40 K min^{-1}. The powder obtained is named S450. In order to compare S450 with H of a similar crystal size, H was calcined at 600 °C in static air for 1 h, applying a heating rate of 40 K min^{-1} (H600).

Powder X-Ray diffraction (XRD) was performed on a Phillips PW 1840 diffractometer equipped with a graphite monochromator using Cu Kα radiation (λ = 0.1541 nm). The Scherrer equation was used to calculate the crystal size of the samples using the (1 0 1) reflection, showing the strongest intensity in the diffractogram.

Transmission electron microscopy (TEM) was performed using a Philips CM30UT electron microscope with a FEG (field emission gun) as the source of electrons operated at 300 kV. Samples were mounted on a Quantifoil microgrid carbon polymer supported on a copper grid.

Nitrogen adsorption and desorption isotherms were recorded on a QuantaChrome Autosorb-6B at 77 K. Samples were previously evacuated at 350 °C for 16 h (at a ramp rate of 10 K min^{-1}). The BJH model was used to calculate the pore size (in this case inter-particle space) distribution from the adsorption branch, and the BET method was used to calculate the surface area (S_{BET}).

The diffuse reflectance infrared Fourier transformed (DRIFT) absorption spectra of the samples were recorded using a Bruker IFS66 spectrometer equipped with a DTGS detector and Spectratech Diffuse Reflectance Accessory including a high-temperature cell. The KBr spectrum was used as background. The stability of surface species formed in a photocatalytic experiment was evaluated as follows. After reaction in the slurry system described later, the spent catalyst was filtered and the recovered powder was dried overnight at 60 °C. The first spectra were recorded at room temperature (RT) under He flow (20 mL min^{-1}), after which the materials were heated to 120 °C and spectra recorded after 1 h equilibration. Subsequently, the samples were heated to 400 °C (10 K min^{-1}). Finally, the materials were cooled down again to room temperature, and the final spectra were recorded. All the spectra were obtained by collecting 128 scans with 4 cm^{-1} resolution.

Thermogravimetric analysis (TGA) of the catalysts before and after reaction was carried out on a TGA/SDTA851e thermobalance (Mettler-Toledo). The sample powders were heated in air from 25 to 900 °C at a heating rate of 10 K min^{-1}.

2.2. Photocatalytic-activity

2.2.1. Slurry reactor

To evaluate catalyst performance in the selective oxidation of cyclohexane, reactions were carried out in a slurry reactor illuminated from the top (the top illumination reactor, TIR), described previously [15] and depicted in Fig. 1A. In a typical experiment, 100 mL of cyclohexane containing 1 g L^{-1} of catalyst was used. The catalysts were dried for 1 h at 120 °C to remove adsorbed water and impurities. The solution was illuminated from the top of the reactor through a Pyrex window that cuts off the highly energetic UV radiation [14]. A high-pressure mercury lamp of 50 W was used (HBO50W from ZEISS). The light intensity of the lamp used in the wavelength absorption range of TiO_2 (275–388 nm) is 55 mW cm^{-2}, which corresponds to 2×10^{-7} Einstein cm^{-2} s^{-1}. Air presaturated with cyclohexane, dried over Molsieve 3 Å, (Acros Organics), was continuously bubbled through the TiO_2 suspension at a rate of 30 mL min^{-1}, ensuring saturation (at a concentration of 0.012 mol L^{-1}). During the reaction, liquid was withdrawn and analyzed by GC. Organic compounds were quantitatively analyzed using a gas chromatograph with a flame ionization detector (Chrompack, CPwax52CB). Hexadecane was used as an internal standard. Unfortunately, calculation of the mass balance is difficult because (i) the reactant is the solvent and the changes in concentration are that small, that the conversion can only be calculated accurately based on product formation and (ii) as shown by ATR-FTIR spectroscopy, the formation of surface carboxylates and carbonates is quite significant, but hard to quantify. Only taking the quantity of cyclohexanone into account, the obtained conversion is estimated at around 2% [8]. For the regeneration experiments, the spent catalyst was filtered, heated

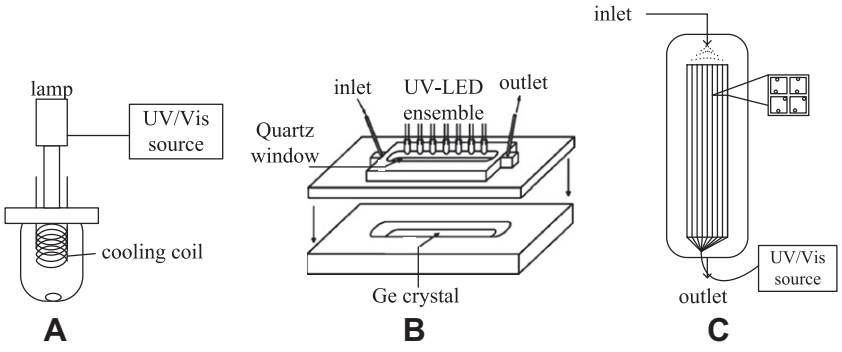

Fig. 1. Schematic representation of the systems used to evaluate the photocatalytic activity: (A) Top Illumination Reactor (TIR); (B) ATR-FTIR system and (C) Internally Illuminated Monolith Reactor (IIMR).

up in static air to 400 °C at 10 K min^{-1}, and treated at this temperature for 1 h. Subsequently, its activity was tested again.

2.2.2. ATR-FTIR

The performance of the catalysts was also evaluated with an *in situ* ATR-FTIR system [17], Fig. 1B. H, H600, and S450 were coated on a Ge ATR crystal. To this end, the catalysts were dried at 120 °C for 1 h in static air and suspended in distilled water at a concentration of 0.85 g L^{-1}. The suspension was treated for 30 min in a 35-kHz Elmasonic ultrasonic bath, after which 2 mL of this suspension was spread on the Ge crystal and dried in vacuum overnight. The conditions used were such to obtain an approximately 1.0-μm-thick coating, as determined by calculations based on anatase density. A volume of 50 mL of cyclohexane (99.0% from J.T. Baker) was used. Cyclohexane was dried over Molsieve (type 4 Å) overnight before use to remove traces of water. Cyclohexane was saturated with O_2 by dry air bubbling at 7.7 mL min^{-1} flow and circulated at 8.8 mL min^{-1} through the ATR cell by means of a high-performance liquid chromatography pump. First, in the dark, adsorption of cyclohexane on the TiO_2 coating at 8.8 mL min^{-1} was monitored. After 90 min, a spectrum of cyclohexane and adsorbed cyclohexane on TiO_2 was collected as background for the photo-oxidation experiments. A mirror velocity of 0.6329 cm s^{-1} and a resolution of 4 cm^{-1} were used for all measurements. UV-induced oxidation of cyclohexane was initiated and continued for 5 h, taking a spectrum every minute. The light was provided by an assembly of 7 UV LEDs with 375-nm wavelength emission with an incident photon flux of 9×10^{-9} Einstein cm^{-2} s^{-1} at the surface of the catalyst coating. The background and the sample spectra were averaged from 64 and 32 scans, respectively.

2.2.3. Structured reactor

A schematic diagram of the internally illuminated monolith reactor (IIMR) is shown in Fig. 1C. The reactor consists of an UV/Vis light source, a standard quartz fiber guide, connected to a specially designed side light fiber bundle, the titania-coated ceramic monolith block (25 cpsi (cells per square inch) and 25 cm long), a liquid inlet with spray nozzle, a gas inlet section and a bottom section for gas–liquid separation and outlet. In order to avoid catalyst loss in macroporosity of the cordierite (monolith material) [14], the monolith was provided with a coating of SiO_2, prior to the coating with S450, as follows. Commercially available SiO_2, Davisil with a mean particle size of 35–75 μm and a pore size of 6 nm, was used for the preparation of a slurry. To this end, 80 g of SiO_2 (IEP = 2) was added under continuous mixing to an HNO_3 (30% v/v)-acidified aqueous solution of pH = 1. The suspension was ball-milled for 24 h, and the final SiO_2 particle size in the slurry was measured in a Malvern Particle Seizer to be ~5 μm (85% of the particles). Prior to the coating, the monolith was dried overnight at 393 K, and after cooling down, the dry monolith was vertically dipped in the slurry for 1 min. The excess of liquid was gently shaken off and further removed out of the monolith channels using a pressurized air knife. Subsequently, the monolith was dried in a warm airflow and calcined at 673 K for 1 h, followed by further heat treatment at 1273 K for 4 h, applying a slow heating rate of 0.5 K min^{-1}. The final SiO_2 coating had a thickness of ~7 μm, after repeating the washcoating procedure twice. The titania paste (S450) was coated on the inside of the square channels of the SiO_2-coated monolith, using the washcoat procedure described for SiO_2, followed by calcination at 723 K for 15 min applying a heating rate of 40 K min^{-1} yielding a catalytic layer thickness of ~5 μm.

Two side light fibers were inserted in each full channel. The original side light fiber bundle, type SLS200T, was supplied by Fibertech GmbH, Berlin, which was designed to have a significant side light emission over a fiber length of 35 cm. In order to enhance the refracted light intensity, the tip of the fiber was polished and coated with a reflective aluminum coating. The UV radiation source was a 100 W mercury short arc lamp (HBO R103W/45, Osram) assembled in a closed case with air cooler, shutter, and timer. The total light intensity emitted from the fibers was of 5.4×10^{-11} Einstein cm^{-2} s^{-1}. The air-saturated liquid cyclohexane with a total volume of 800 ml was recirculated at 330 mL min^{-1} through a reservoir and the reactor with a variable speed gear pump, and the flow was measured via a turbine flow sensor.

The temperature was maintained at room temperature using an external thermostat. The spray nozzle distributed the liquid over the monolith, of which the distance between nozzle tip and the monolith was so adjusted that an even distribution of liquid over the channel walls was achieved. During reaction, liquid samples were taken and analyzed using a gas chromatograph with a flame ionization detector (Chromopack, CPwax52CB). Quantification of the oxygenated products in the liquid phase was derived from a multipoint calibration against the internal standard.

3. Results

3.1. Catalyst characterization

In Fig. 2, the XRD patterns of H, H600, and S450 are depicted, indicating that all three catalysts consist of anatase. S450 shows a much higher crystallinity than H, as evidenced by the width and amount of characteristic lines present in the diffractogram. Due to calcination, the H600 material presents a better defined XRD pattern of anatase than H, but the diffraction lines are still less well defined and sharp when compared to S450. From the Scherrer equation, the crystal diameters were calculated to be 7 nm, 19 nm, and 20 nm for H, H600, and S450, respectively.

The surface area of the materials was determined by N_2-physisorption, and the values obtained with the BET method were 330 m^2 g^{-1} for H, 73 m^2 g^{-1} for H600, and 80 m^2 g^{-1} for S450. The isotherms and pore size distribution are depicted in Fig. 3a and b, respectively. S450 exhibits a pore size distribution with a maximum at ~13 nm (mesoporous), attributed to well-defined and ordered inter-particle spaces. In the case of H and H600, the pore size distribution is not so well defined and is very broad with maxima at less than 5 nm in size for H and between 5 and 10 nm for H600 also attributed to inter-particle spaces. The absence of hysteresis, as shown in Fig. 3a, is in agreement with this type of (micro)porosity.

In Fig. 4, the TEM micrographs of the materials under study are shown. The pictures show that H, Fig. 4a, consists of nano-TiO_2 crystallites, connected to form a porous network; the nanoparticles

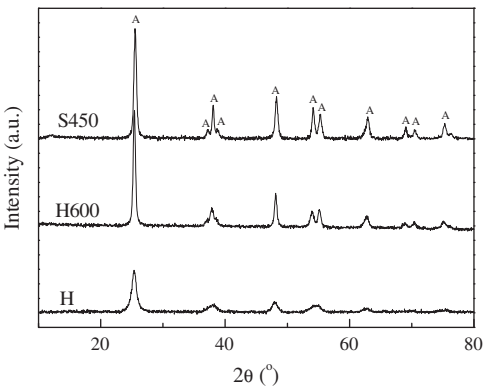

Fig. 2. XRD patterns of H, H600 and S450. The anatase peaks are indicated by A.

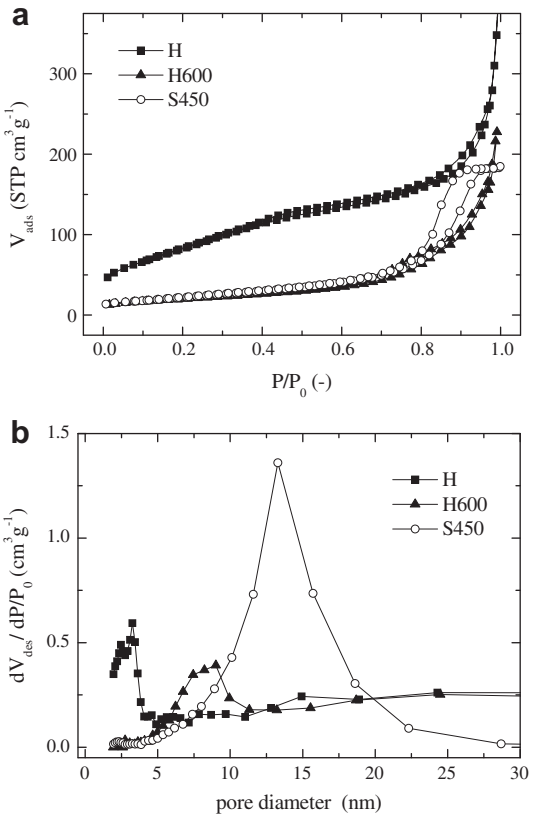

Fig. 3. Textural analysis of H, H600 and S450: (a) N_2-physisorption isotherms and (b) pore size distribution.

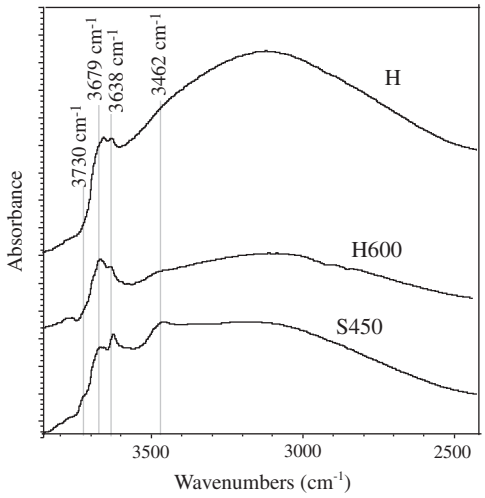

Fig. 5. IR spectra of the catalysts used in this study H, H600 and S450. The most important IR bands assigned to various surface OH groups are indicated.

are not well-defined separated crystallites. The observation of a porous network is in agreement with the N_2-physisorption results, which suggest that porosity originates from inter-particle spaces. Most of the crystalline grains are spherical, and the average crystallite size is 5 nm (3.5–7 nm) in agreement with the value determined by the Scherrer equation. Fig. 4b shows the micrograph of H600. Apparently, calcination leads to a clear increase in the primary particles to a range between 15 and 30 nm, centered at 20 nm. Although extensive sintering has occurred, the particle shape is still not well defined, and the individual particles are still largely agglomerated, as shown in the inset of Fig. 4b. The morphology of S450, Fig. 4c, is very different from both H and H600. It is made up from monocrystalline nanoparticles that exhibit shapes mostly related to polygons (truncated squares or rectangles) presenting defined crystal faces, although some spherical-like particles without well-defined crystal faces can also be observed. The particle size distribution ranges from 8 to 50 nm and is centered at 22 nm.

The IR spectra of the materials studied are depicted in Fig. 5. In the region of 4000–2500 cm^{-1}, O—H stretching modes are located. The band at 3730 cm^{-1} is assigned to an isolated anatase OH vibration, and the bands at 3679 cm^{-1} and 3638 cm^{-1} are assigned to bridging OH groups, $(Ti)_2$–OH, of anatase [20–23]. The bridging OH groups are neighboring sites and bind to each other by hydrogen bridges [20]. In the S450 spectrum, these bands are more clearly resolved, especially the band at 3638 cm^{-1}, probably due to a lower amount of adsorbed water [22]. The spectral contributions of physisorbed water are present in the region 3500–2500 cm^{-1} with maxima at 3100 cm^{-1}, 3462 cm^{-1}, and 3600 cm^{-1} [24,25]. When the amount of water is high, normally the bands at 3462 cm^{-1} and 3600 cm^{-1} cannot be resolved, as in the case of H. The band at 3462 cm^{-1} is clearly resolved in S450 and H600, which implies again a lower quantity of surface-adsorbed water for H600 and S450.

3.2. Photocatalytic-activity

In Fig. 6, the reaction profiles for the formation of cyclohexanone are depicted. Initially, the rates for H600 and S450 are comparable, while H exhibits a slightly higher rate, as illustrated by the inset of Fig. 6. The rate of product formation starts to decrease

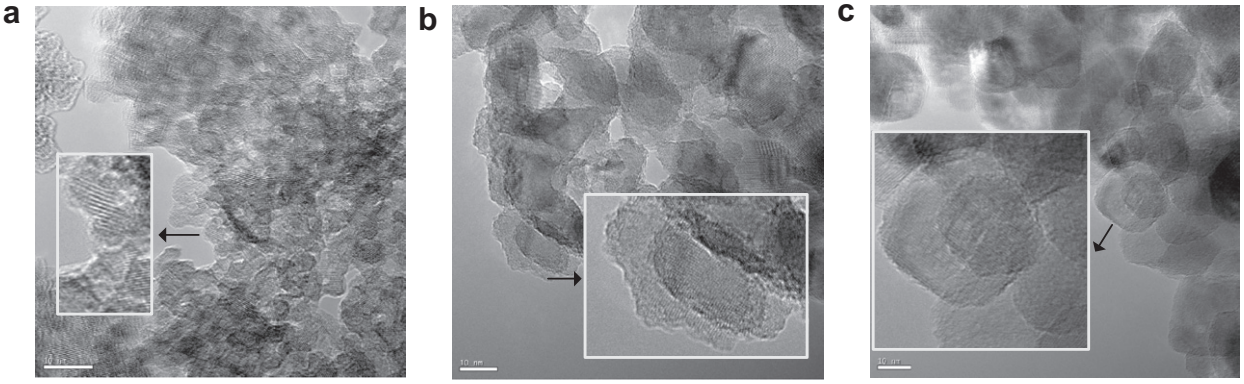

Fig. 4. TEM micrographs of (a) H (b) H600 and (c) S450. The insets show magnification of the indicated picture area.

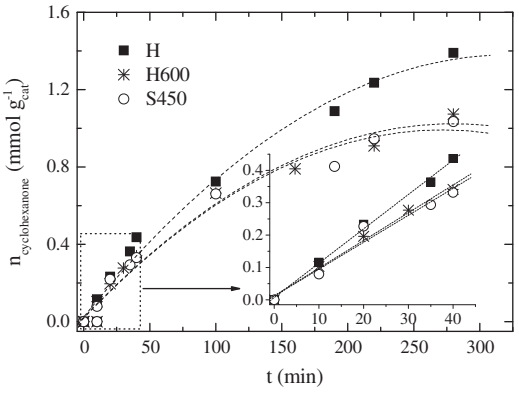

Fig. 6. Cyclohexanone formation as a function of time for H, H600 and S450, as determined in the top illumination reactor.

after approximately 50 min, obviously due to deactivation, until a plateau is reached and the production stops. The productivity toward cyclohexanone is highest for H, followed by H600 and S450, which have very similar production curves.

TGA measurements of the fresh and spent catalysts are shown in Fig. 7. For the fresh materials, similar TGA profiles were obtained previously and interpreted as follows [26]. The peak at ~60 °C corresponds mostly to weakly adsorbed water, the second peak at higher temperatures at ~200 °C is assigned to water closer to the surface (increasing adsorption strength) and associated with dehydroxylation. For the fresh materials (*i.e.* before reaction), the weight loss at 60 °C is one order of magnitude higher for the H material, when compared to H600 and S450. For the spent catalysts (*i.e.*, after reaction), the weight loss at 60 °C decreases for all the materials, but less severely in the case of H600. The water desorption feature at T_r = 200 °C clearly increases for S450, indicating an increase in the degree of hydration induced by the photocatalytic reaction.

To further evaluate differences in surface chemistry of the TiO_2 samples under investigation, Fig. 8 shows the ATR-FTIR spectra recorded during reaction. In order to visualize the surface chemistry, Fig. 9 is presented. It is stated in the literature that when cyclohexanone is formed at the surface, it can follow two routes: desorption to the reaction medium (cyclohexane) or further oxidation to carboxylates, carbonates and finally to CO_2/H_2O. It is also claimed that besides this pathway involving cyclohexanone, a non-selective route of cyclohexylperoxide decomposition to carboxylates and carbonates exists. The formation of carbonates and carboxylates through the aforementioned routes is claimed to be responsible for the deactivation of OH groups on the TiO_2 surface.

In Fig. 8a, the spectral development during reaction of the H sample is shown, which is in agreement with data previously reported by Almeida et al. [17]. After 5 min of reaction, formation of species at the catalyst surface is already apparent. A broad range of infrared absorptions develops in time between 1800 and 1000 cm^{-1}, consisting of several overlapping bands.

Cyclohexanone formation can be followed by the band at 1714 cm^{-1}, which corresponds to the C=O stretching vibration of bulk cyclohexanone, and at 1690 cm^{-1}, corresponding to the C=O stretching vibration of adsorbed molecules [17]. The peak at 1575 cm^{-1} is assigned to C=O stretching vibrations of adsorbed carboxylates [27,28]. The adsorbed carbonate species are located in the spectra at 1403 cm^{-1} [28,29]. Various smaller bands can be observed below 1400 cm^{-1} which can be assigned to the C—H bending modes of bulk and adsorbed cyclohexanone, as well as to carboxylates. The spectra of H600 (Fig. 8b) and S450 (Fig. 8c), show qualitatively the same bands as present in the spectra of H, but the intensities are different. In particular, the relative absorption intensity of cyclohexanone (1714 and 1690 cm^{-1}) over

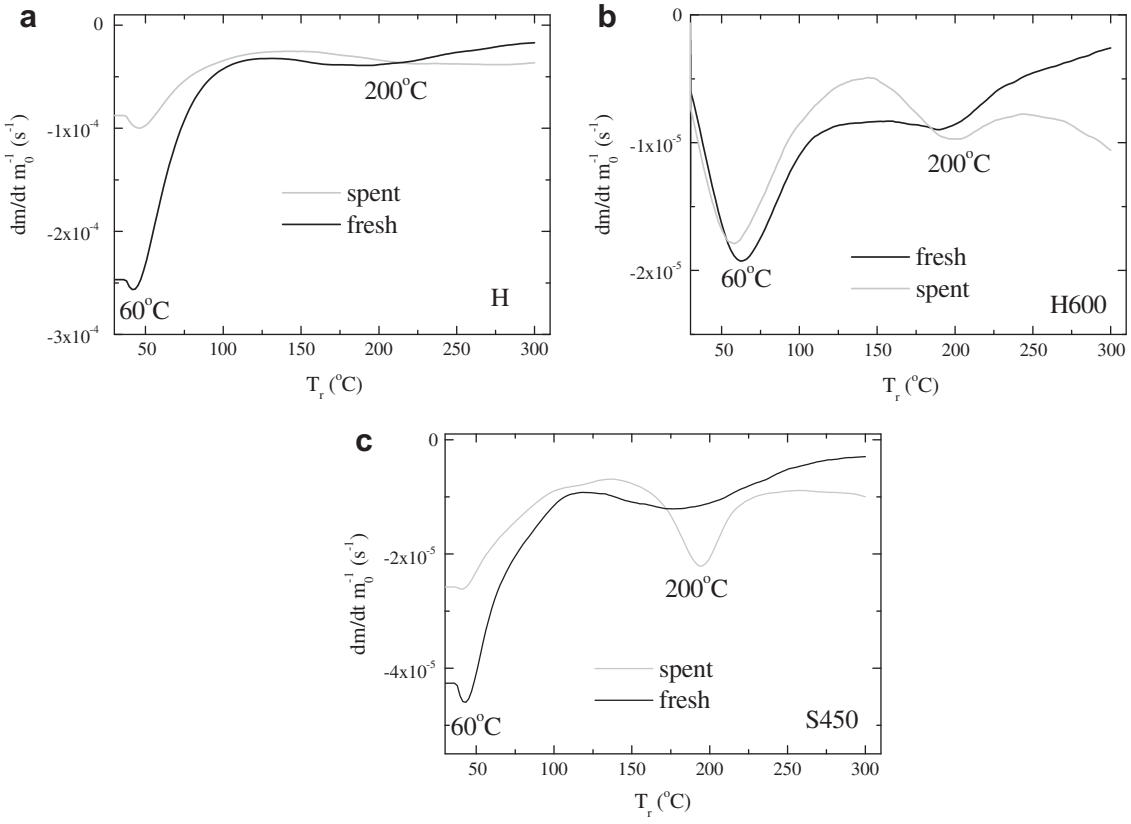

Fig. 7. TGA results for the fresh samples (black lines), and after reaction, presented as weight change in time *vs* reference temperature (T_r). (a) H, (b) H600, and (c) S450.

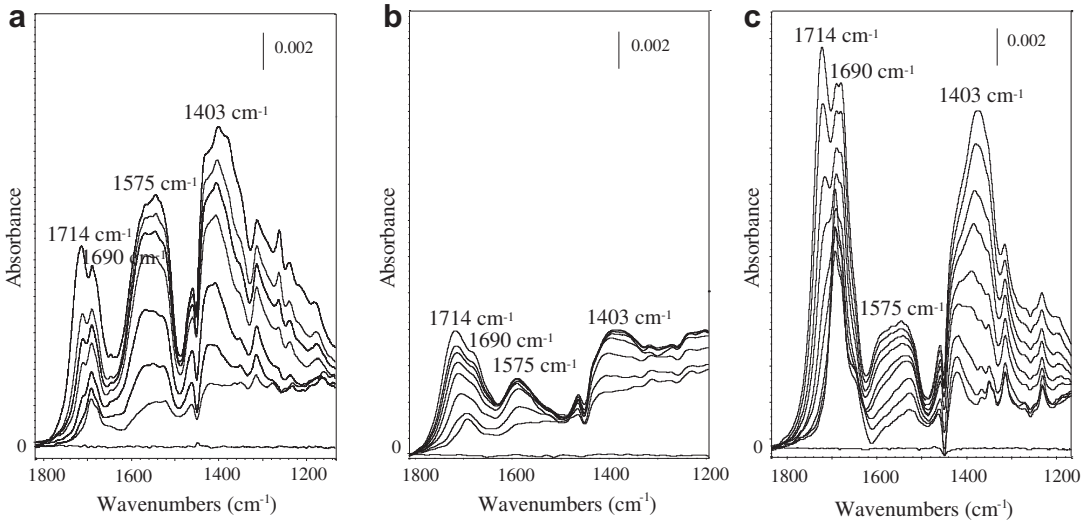

Fig. 8. *In situ* ATR-FTIR spectra of cyclohexane photocatalytic oxidation over (a) H, (b) H600 and (c) S450. Spectra were recorded in the time range of 0.5–240 min. The wavenumbers of the most important bands are indicated: 1714 and 1690 cm^{-1} for bulk and adsorbed cyclohexanone, respectively, 1575 cm^{-1} representing carboxylates, and 1403 cm^{-1} carbonates.

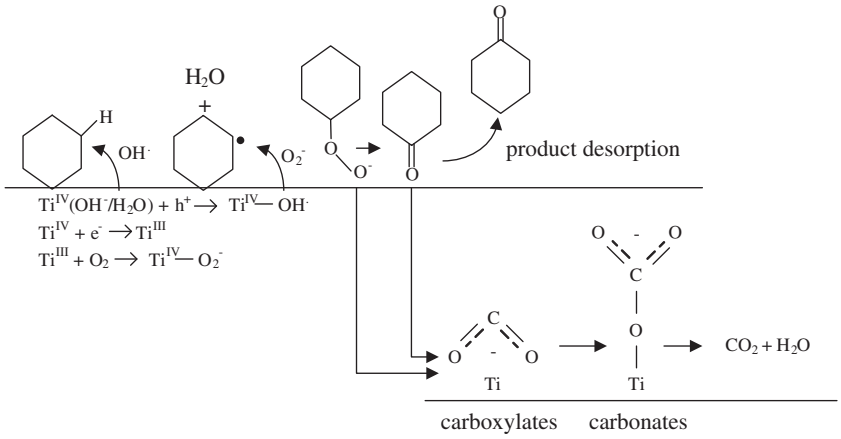

Fig. 9. Surface reaction mechanism of the photocatalytic oxidation of cyclohexane (based on [17]). The carbonate and carboxylate species are formed by consecutive oxidation of the intermediate peroxide and the product cyclohexanone. The photon-induced chemistry of TiO_2 is also presented.

carboxylates (1575 cm^{-1}) is a strong function of the catalyst applied, in agreement with previous studies [30]. In addition, the development of the intensity of the IR absorptions of adsorbed water centered at 3375 cm^{-1}, and of the most acidic OH groups, bridged OH groups, referred to as $(Ti)_2$–OH, located at 3633 cm^{-1}, is quite different for the various catalyst materials [31], as shown in Fig. 10. The surface coverage of H with water is increasing in the first 20 min of reaction, followed by a continuous decrease until a minimum plateau with negative absorption values is reached. This suggest that surface-adsorbed water present *prior* to the experiment has been desorbed. For H600, water formation and $(Ti)_2$–OH conversion is less pronounced, as expected on the basis of the lower surface area of H600 when compared to H. Surprisingly, water formation is much more significant in the initial stages of the reaction when S450 is applied as photocatalyst, as shown in Fig. 10c. Eventually negative absorption values are obtained. The $(Ti)_2$–OH intensity decreases in all three cases: strongest for S450, followed by H and finally by H600.

Finally, significant differences were found for the three catalysts in the time-dependent development of the ratio of adsorbed *vs* bulk cyclohexanone. The left side of Fig. 11 shows the spectra in the region where the absorption bands of bulk (~1714 cm^{-1}) and adsorbed (1780 and 1790 cm^{-1}) cyclohexanone are located. Using deconvolution of these bands, absorption values were calculated. These were subsequently used to calculate the amount of cyclohexanone produced, corrected for the amount of catalyst present in the coating, and taking the different light intensity used in the TIR and ATR-FTIR into account [18]. A linear correlation was assumed between the data from the TIR (corresponding to the amount of bulk cyclohexanone formed) and the peak area in the ATR-FTIR. The values for adsorbed cyclohexanone were calculated on the basis of the same correlation, assuming that the relative molar absorption coefficients of adsorbed and bulk cyclohexanone are similar.

Clearly, for all catalysts, the time profiles show that in the first 10 min predominantly adsorbed cyclohexanone is formed at a high rate. This is followed by a much slower rate in the subsequent time range of the experiment. The rate of formation of bulk cyclohexanone is initially lower than that of surface-adsorbed cyclohexanone, but is rather constant, leading to a higher rate for the formation of bulk *vs* adsorbed cyclohexanone formation in the final stages of the experiment. This nicely shows that the process is a serial reaction, *viz.*, formation at the surface followed by desorption. The initial rate of formation of adsorbed cyclohexanone increases in the order H600 < H < S450; the trends in the initial rate of

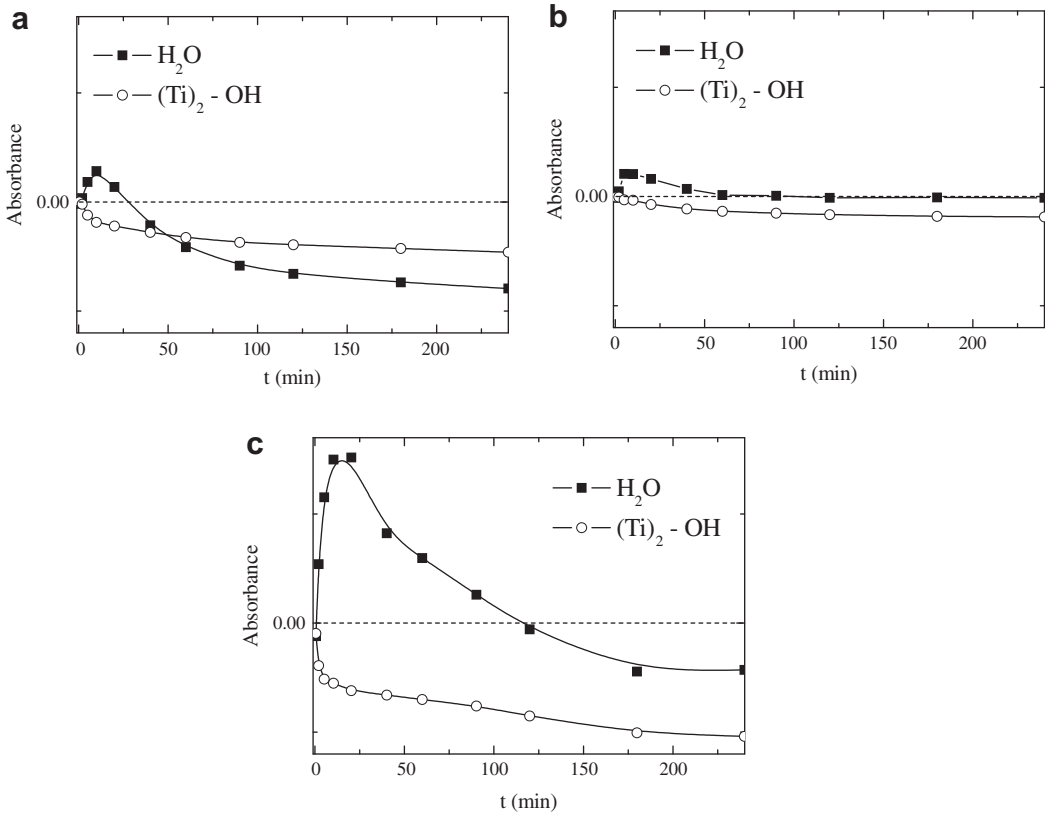

Fig. 10. Time evolution of selected bands from the spectra measured with the ATR-FTIR system for (a) H, (b) H600, and (c) S450. Adsorbed water (based on the band centered at 3375 cm^{-1}) and bridged $(Ti)_2$–OH group (assumed to be the 3633 cm^{-1} absorption). Note: the scale of the absorption axis is the same for all three cases.

formation of bulk cyclohexanone are comparable to the TIR results. However, the light intensity used in the *operando* ATR experiments was 20 times smaller than used in the TIR reactor and therefore the rates (and amounts) as well [18].

The amount of adsorbed cyclohexanone formed during reaction is plotted as a function of the bulk cyclohexanone concentration in Fig. 12. For the three materials, two plateaux are observed, indicated as a and b. These values correspond to 0.02 mmol g_{cat}^{-1} for H, 0.01 mmol g_{cat}^{-1} for H600, and 0.07 mmol g_{cat}^{-1}, for S450, respectively. It should be noted that these curves should not be considered as equilibrium isotherms.

After reaction, the spent H and S450 catalysts were analyzed in a DRIFT system at different temperatures to evaluate the possibility of regeneration by a high-temperature treatment. The series of spectra obtained at room temperature (RT), 120 °C, 400 °C, and after subsequent cooling down to room temperature (RT2) are shown in Fig. 13. For both spent catalysts, there are several absorptions visible in the wavenumber region of 1800–1000 cm^{-1}, assigned to the carboxylate/carbonate species. The insets show the values of the total integrated peak area of the carbonate and carboxylate absorptions. In the case of H, Fig. 13a, heat treatment at 400 °C did not lead to a significant reduction in integrated peak area, whereas in the case of S450, Fig. 13b, significant decomposition of surface carbonates and carboxylates was observed. The spectrum of S450 (RT2), obtained after cooling down to room temperature, is quite similar to the spectrum of the fresh material shown in Fig. 5, suggesting full regeneration.

In order to check whether the heat treatment of S450 at 400 °C indeed restores the catalytic activity, tests were conducted in the TIR. Fig. 14 shows the initial cyclohexanone formation for the fresh catalysts and for the same materials after reaction and heat treatment at 400 °C for 1 h. For H and H600, the activity could not be restored by heat treatment, as predicted by the previous DRIFT studies, but in the case of the S450 catalyst the activity and selectivity (defined here as cyclohexanone/cyclohexanol ratio) are completely restored after heat treatment of the used catalyst.

To confirm the feasibility of the S450 catalyst in (semi-)continuous operation, cyclohexanone and cyclohexanol formation over S450 paste coated on the walls of a ceramic monolith was evaluated. Fig. 15 shows the high performance of the catalyst, with only slight deactivation during 4 h of operation. Subsequently, the monolith containing the catalyst was heated at 400 °C for 1 h after the 1st run and tested again in a 2nd run. Photoactivity was found to be exactly the same in the two experiments, confirming that the conditions of the rejuvenation procedure do not deteriorate catalytic performance.

An overview of the photonic efficiencies for the materials in the different reactors used in this study is given in Table 1. The photonic efficiency was determined using the following equation [18]:

$$\xi = \frac{\text{Reaction rate (mol s}^{-1})}{\text{Photon flow (Einstein s}^{-1})} = \frac{dn/dt}{AI''}$$

In this equation, n is the number of moles converted (mol), t the time (s), A the area through which light propagates into the reactor (m^2), and I'' the photon flux (Einst m^{-2} s^{-1}). The values presented show that the highest efficiency is obtained for S450 material in the ATR-FTIR with a value of 0.018. These values are small but in agreement with values reported previously [18].

4. Discussion

4.1. Product distribution and catalyst deactivation

In situ ATR-FTIR gives direct information on the chemical nature of the adsorbed species formed during reaction. The spectra in

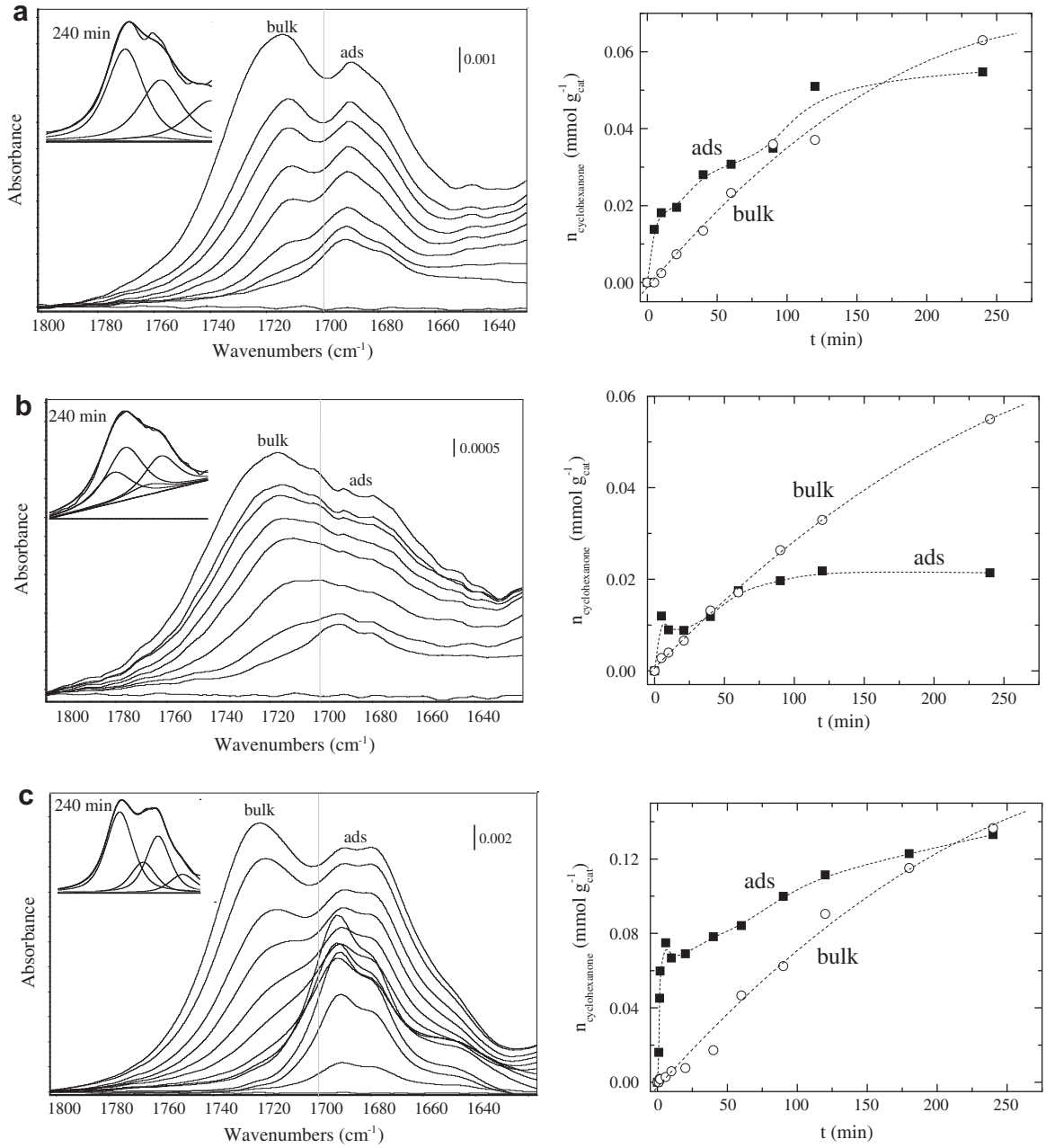

Fig. 11. Development of absorption bands of bulk (1714 cm^{-1}) and adsorbed (1690 and 1680 cm^{-1}) cyclohexanone as a function of time, and the corresponding intensity profiles obtained by peak deconvolution for (a) H, (b) H600, and (c) S450.

Fig. 8 show that the ratio of the sum of adsorbed (1690 cm^{-1}) and desorbed (1714 cm^{-1}) cyclohexanone over carboxylates (1575 cm^{-1}) and carbonates (1403 cm^{-1}) decreases in the series S450 > H600 ≫ H. In particular, for S450 and H600, the carboxylate concentration is relatively small when compared to H. This observation can be explained considering time-resolved microwave conductivity measurements reported previously: the electron lifetime and mobility upon illumination is highest for S450, followed by H600 and H [32,33]. The opto-electronic properties are related to the crystal quality of the material: less crystal defects and thus less amount of electron trapping sites within the crystal lead to higher electron mobility, suggesting higher concentration of holes available for OH radical formation. The OH radicals induce a high photocatalytic activity toward the selective formation of cyclohexanone [30,34] but can also contribute to consecutive oxidative processes, in particular the consecutive oxidation of carboxylates to carbonates (and CO_2), cleaning and regenerating the active sites. This explains the surprisingly low differences in catalytic activity despite the large difference in surface area (which is much higher for H when compared to H600 and S450) and the high extent of consecutive oxidation of carboxylates to carbonates (and likely CO_2).

4.2. Water formation

According to the mechanism reported in Fig. 9, water is formed in two stages of the reaction: upon formation of the cyclohexyl radical and when complete oxidation takes place. The water formation in the beginning of the reaction, Fig. 10, is also reflected by the decreasing intensity in the IR spectrum of the features of $(Ti)_2$–OH sites; this decrease is largest for S450 followed by H and finally H600. The decrease is probably caused by hydrogen bonding with

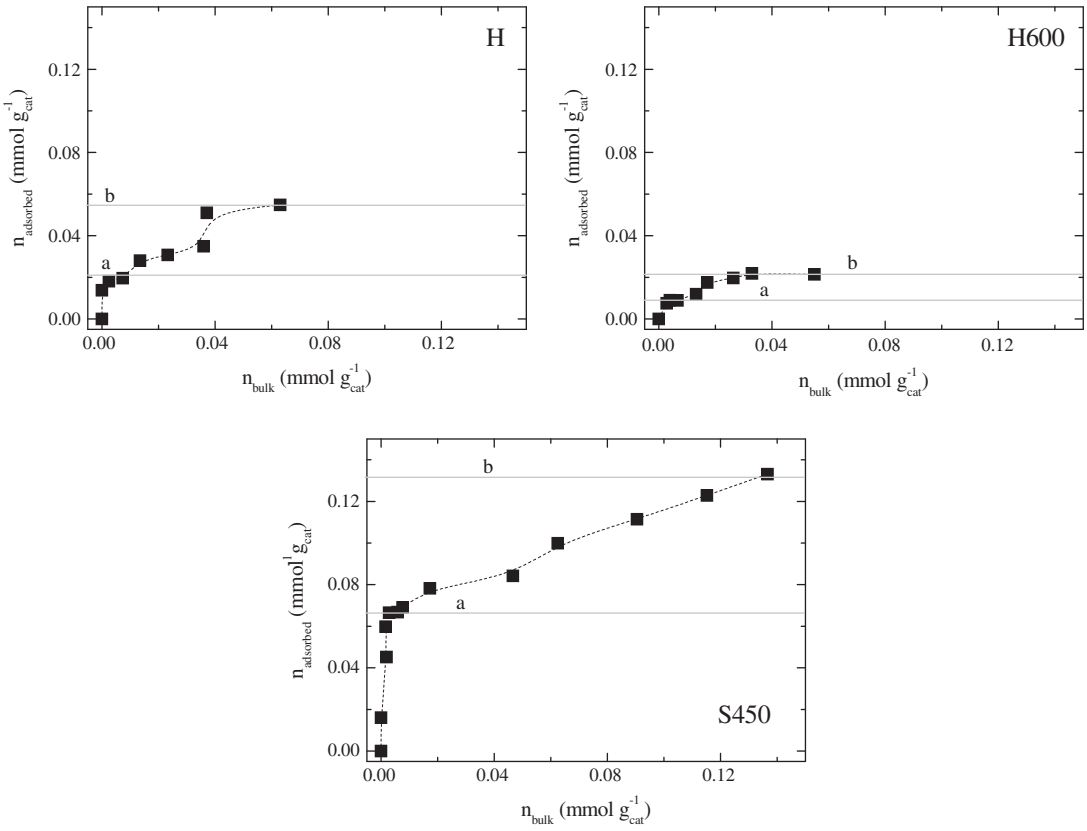

Fig. 12. Changes in adsorbed cyclohexanone concentration as a function of changes in bulk concentration caused by the reaction. Deconvoluted band areas of adsorbed and bulk species were converted to bulk and surface concentrations as indicated in the text. For each plot, two adsorption *plateaux* can be identified, indicated as 'a' and 'b'.

surface-adsorbed cyclohexanone and water, which would lead to a red shift of the O—H absorption modes [35]. The net consumption of surface-adsorbed water observed in later stages of the reaction, as shown in Fig. 10, is likely due to a combination of a relatively low cyclohexane oxidation rate, water desorption, and occupation of adsorption sites by the carboxylates and carbonates formed. Furthermore, water decomposition into hydroxyl radicals might contribute [17]. The changes in spectral intensities in the >3000 cm^{-1} region follow the order H > S450 > H600. The trend in the decreasing TGA peak at 60 °C, corresponding to the outermost layer with the most labile adsorbed water [36], is in agreement with the ATR observations. This water is likely adsorbed from the laboratory environment in the time between the photocatalytic and TGA experiments. TGA data also show that the peak at 200 °C, assigned to strongly surface-bound water, increases strongest in the case of the S450, slightly for H600, while for H the difference is within the error of measurement. This suggests that in the initial stages of the photocatalytic reaction on S450 strongly bound water is contributing to the changes in spectral intensities, which is also largely increased.

4.3. Adsorbed vs bulk cyclohexanone

The spectra recorded during reaction allow to differentiate between the rate of formation at the catalyst surface and the rate of desorption of cyclohexanone to the reaction bulk. Fig. 12 shows very different patterns for the three systems. For all materials, the rate of formation of adsorbed cyclohexanone is initially highest, in particular for S450.

For the interpretation of these observations, we considered the following possibilities:

- series reaction behavior, implying non-equilibrium adsorption,
- multilayer adsorption, with the interference of deactivating species,
- adsorption models based on two types of adsorption sites,
- formation of new sites during reaction.

The various options will be discussed subsequently in the following. Series reaction behavior, implying non-equilibrium adsorption, can be discarded, since this would lead to a maximum, due to consecutive cyclohexanone consumption, which is not experimentally observed (Fig. 12). The second interpretation, multilayer adsorption, seems in agreement with the staircase shape that occurs normally for multilayer adsorption on non-porous surfaces. Whether this interpretation is feasible depends on various factors. First, it is important to evaluate whether the number of adsorbed molecules is comparable to the amount of adsorption sites, *i.e.*, surface OH groups. These have been determined by NH_3-TPD for the three materials and amount to 1.15 mmol g_{cat}^{-1} for H, 0.43 mmol g_{cat}^{-1} for H600, and 0.40 mmol g_{cat}^{-1} for S450. Furthermore, the final value of the amount of cyclohexanone produced (plateau b in Fig. 12) should be estimated. This amount is difficult to assess quantitatively, and the values given in Fig. 12 should only be regarded as in indication of the order of magnitude in view of uncertainties in (i) molar absorption coefficient of adsorbed cyclohexanone, (ii) peak area determination with associated deconvolution errors, and (iii) that a factor of 20 lower light intensity leads to a 20 times lower amount of product [18]. Given these uncertainties, the amount of surface-adsorbed cyclohexanone is much lower than the values estimated for the amount of OH groups (0.02 mmol g_{cat}^{-1} for H, 0.01 mmol g_{cat}^{-1} for H600, and 0.07 mmol g_{cat}^{-1} for S450). Multilayer adsorption is therefore not

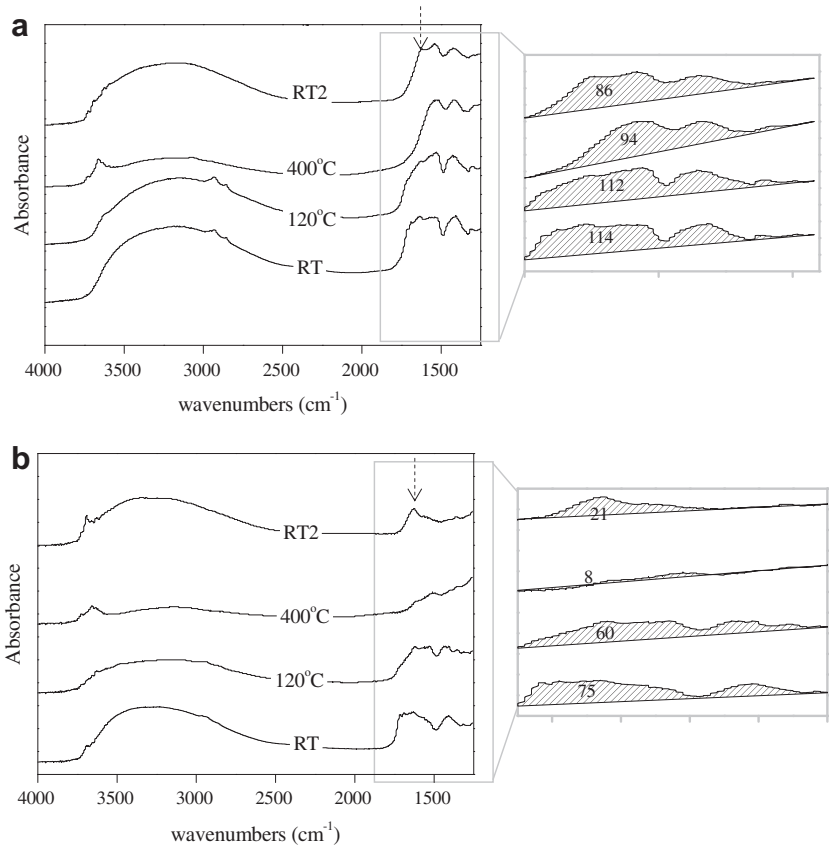

Fig. 13. DRIFT spectra of the spent materials (a) H and (b) S450 during various steps in the regeneration process. The first spectrum is recorded of the spent catalyst at room temperature (RT), then the sample is heated to 120 °C and subsequently to 400 °C; finally, it is cooled down to room temperature (RT2). The arrows indicate the low-frequency band of adsorbed water at 1630 cm^{-1}. The insets are a zoom out of the carboxylate/carbonate region (1700–1300 cm^{-1}), with the corresponding values of the area under the peak indicated.

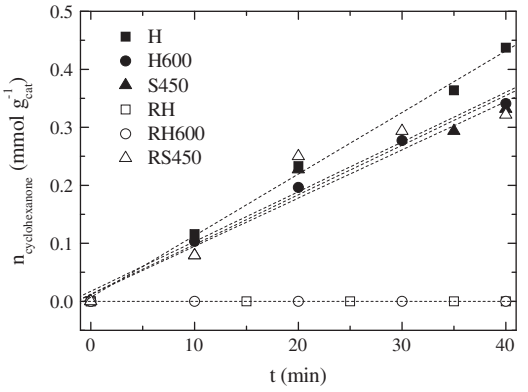

Fig. 14. Cyclohexanone formation in the first 40 min of reaction, obtained in the TIR using fresh catalysts: H, H600, and S450 and spent catalysts after heat treatment in air at 400 °C: RH, RH600, and RS450 with the proceeding R indicating "regenerated".

very likely. Also a monolayer adsorption is unlikely: in view of the large amounts of carboxylates and carbonates formed, it would *a priori* be impossible to create a monolayer of adsorbed cyclohexanone molecules during reaction. Finally, it should be noted that the amount of surface cyclohexanone (and carbonate) produced in the ATR cell is remarkably large for S450 in comparison with H600. This requires further investigation.

A two-site model might also explain the data presented: one site that gives very strong adsorption (a) and the other a weaker adsorption (b). A two-site model is in fair agreement with the two absorption frequencies found for adsorbed cyclohexanone at 1690 and 1680 cm^{-1}. Furthermore, the rapid loss in spectral intensity of the $(Ti)_2$–OH in the initial stages of the experiment suggests that these are rapidly completely occupied. Another OH group of which the identity cannot be determined from the ATR data might account for the remaining activity. In particular, in the case of Solaronix, a *plateau* is not reached for b, however. Since equilibrium is not reached for these sites, the production at the surface and subsequent desorption occurs in series. Furthermore, the concentration of adsorbed cyclohexanone is increasing and we tentatively explain this observation by assuming that new OH sites are being formed by decomposition of water produced during the reaction. This type of mechanism has been reported to occur at an oxygen defect site: one OH group doubly coordinated to Ti atoms at the oxygen defect site converts under light illumination by interaction with a water molecule to two OH groups, singly coordinated at each Ti atom [37]. Furthermore, it has been shown that rehydroxylation is successful in highly crystalline TiO_2, such as in S450, whereas this is not the case when a high percentage of amorphous phase is present, such as in H [20].

4.4. Catalyst regeneration by heat treatment

Undoubtedly, catalyst regeneration is essential to make any commercial implementation of photo-oxidation of cyclohexane feasible. Results show that for the three materials studied, the formation of carboxylates and carbonates (*i.e.*, deactivating species) is evident in the first initial moments of the reaction together with the adsorbed cyclohexanone. It has been reported that

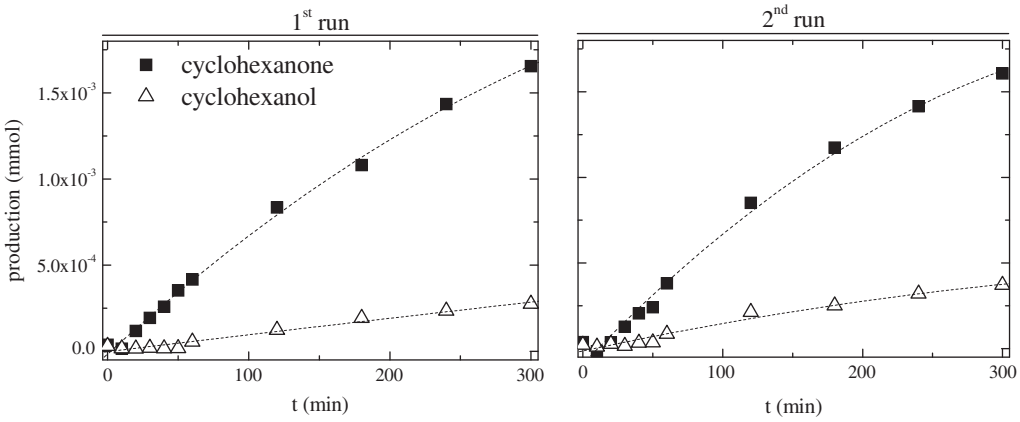

Fig. 15. Cyclohexanone and cyclohexanol production as obtained in the IIMR: the 1st run is representative of a fresh coating of S450, and the 2nd run of the spent coating, regenerated by calcination at 400 °C.

Table 1
Overview of photonic efficiencies determined for each reactor and material used in this study.

	ξ (mol Einst^{-1})		
	H	H600	S450
TIR	0.005	0.004	0.004
ATR-FTIR	0.006	0.006	0.018
IIMR	–	–	0.010

carboxylates and carbonate formation is due to further oxidation not only of cyclohexanone but also of other intermediates and products such as cyclohexylperoxides and cyclohexanol [17]. Clearly, it is very difficult if not impossible to completely avoid their formation, and as a consequence, it is crucial to remove them without irreversible loss of activity of the catalyst. The amount and chemical distribution of the species adsorbed after the reaction are quite different for the three catalysts. Carbonates are dominant on S450, with hardly any carboxylates present, while for H both carbonate and carboxylate species are extensively present at the surface. While this difference in chemical nature might partly explain the observed regenerability of S450 and the irreversible deactivation of H and H600, also the thermal stability of the (same) adsorbed species is quite different, as demonstrated by the DRIFT experiment. This might be associated with the amount of defects/irregularities on the crystal surfaces of H and H600 observed in the TEM measurements. Clearly, the morphology of S450 consists of smooth crystal surfaces, which implies less corner and step sites. At these sites, present in H600 and H, the thermal stability of surface-adsorbed species is likely to be higher, explaining the differences in thermal decomposition/removal rates [38]. The conclusion is that not only the bulk structure of the catalyst needs to contain no, or in any case only small amounts of defects, inducing favorable opto-electronic properties and thus limiting carboxylate formation, but also the surface should consist of defect-free planes, decreasing (thermal) stability of adsorbed species, allowing thermal regeneration procedures. Solaronix TiO_2 has these properties to a larger extent than H and H600 and is therefore better to regenerate and more promising for application in slurry and in particular immobilized reactors. Further studies with this material, especially evaluating the application of water in the feed, are ongoing.

5. Conclusions

Hombikat as received (H) shows the highest rate of cyclohexanone formation in photocatalytic oxidation of cyclohexane in a Top Illumination Reactor, compared to H600 (Hombikat calcined at 600 °C) and Solaronix S450. All catalysts suffer from deactivation. However, deactivation of H and H600 was found to be irreversible, due to a high thermal stability of surface-adsorbed carbonates and carboxylates. For S450, the surface population after photocatalytic reaction (ratio of carboxylates over carbonates) was different, and thermal stability of these species was found to be significantly lower, which allowed regeneration of this material by heat treatment in air at 400 °C. The regenerated S450 catalyst was successfully used both in slurry (Top Illumination Reactor) and in immobilized applications (Internally Illuminated Monolith Reactor). In particular, for the latter reactor configuration, regenerability is a desired property. The high catalyst stability of materials such as S450 is an important first step toward the practical application of photocatalysis in selective liquid-phase photo-oxidation processes.

Acknowledgments

We would like to acknowledge the X-ray facilities of the Faculty 3ME, of the Delft University of Technology, for the X-Ray analyses. Indra Puspitasari and Ugo Lafont of DCT/NCHREM, Delft University of Technology, are acknowledged for performing the TEM measurements. STW (VIDI Project DPC.7065) is gratefully acknowledged for financial support.

References

[1] O. Carp, C.L. Huisman, A. Reller, Prog. Solid State Chem. 32 (2004) 33–177.
[2] M.R. Hoffmann, S.T. Martin, W.Y. Choi, D.W. Bahnemann, Chem. Rev. 95 (1995) 69–96.
[3] M. Schiavello, Heterogeneous Photocatalysis, Wiley, Chichester, 1997.
[4] A. Maldotti, A. Molinari, R. Amadelli, Chem. Rev. 102 (2002) 3811–3836.
[5] A.K. Suresh, M.M. Sharma, T. Sridhar, Ind. Eng. Chem. Res. 39 (2000) 3958–3997.
[6] C.B. Almquist, P. Biswas, Appl. Catal. A - Gen. 214 (2001) 259–271.
[7] P. Boarini, V. Carassiti, A. Maldotti, R. Amadelli, Langmuir 14 (1998) 2080–2085.
[8] P. Du, J.A. Moulijn, G. Mul, J. Catal. 238 (2006) 342–352.
[9] C. Giannotti, S. Legreneur, O. Watts, Tetrahedron Lett. 24 (1983) 5071–5072.
[10] J.M. Herrmann, W. Mu, P. Pichat, Stud. Surf. Sci. Catal. (1991) 405–414.
[11] G.X. Lu, H.X. Gao, J.H. Suo, S.B. Li, J. Chem. Soc. Chem. Commun. (1994) 2423–2424.
[12] W. Mu, J.M. Herrmann, P. Pichat, Catal. Lett. 3 (1989) 73–84.
[13] M.A. Brusa, M.A. Grela, J. Phys. Chem. B 109 (2005) 1914–1918.
[14] P. Du, J.T. Cameiro, J.A. Moulijn, G. Mul, Appl. Catal. A – Gen. 334 (2008) 119–128.
[15] J.T. Carneiro, C.C. Yang, J.A. Moma, J.A. Moulijn, G. Mul, Catal. Lett. 129 (2009) 12–19.
[16] M.A. Brusa, Y. Di Iorio, M.S. Churio, M.A. Grela, J. Mol. Catal. A - Chem. 268 (2007) 29–35.
[17] A.R. Almeida, J.A. Moulijn, G. Mul, J. Phys. Chem. C 112 (2008) 1552–1561.

[18] J.T. Carneiro, R. Berger, J.A. Moulijn, G. Mul, Catal. Today 147 (2009) S324–S329.
[19] C.J. Barbe, F. Arendse, P. Comte, M. Jirousek, F. Lenzmann, V. Shklover, M. Gratzel, J. Am. Ceram. Soc. 80 (1997) 3157–3171.
[20] M. Primet, P. Pichat, M.V. Mathieu, J. Phys. Chem. 75 (1971) 1216.
[21] M. Primet, P. Pichat, M.V. Mathieu, J. Phys. Chem. 75 (1971) 1221.
[22] J.A.R. Vanveen, F.T.G. Veltmaat, G. Jonkers, J. Chem. Soc. Chem. Commun. (1985) 1656–1658.
[23] A.S. Vuk, R. Jese, M. Gaberscek, B. Orel, G. Drazic, Sol. Energy Mater. Sol. Cells 90 (2006) 452–468.
[24] M.A. Henderson, Surf. Sci. 355 (1996) 151–166.
[25] M.A. Henderson, Langmuir 12 (1996) 5093–5098.
[26] T. Lopez, E. Sanchez, P. Bosch, Y. Meas, R. Gomez, Mater. Chem. Phys. 32 (1992) 141–152.
[27] P.Z. Araujo, C.B. Mendive, L.A.G. Rodenas, P.J. Morando, A.E. Regazzoni, M.A. Blesa, D. Bahnemann, Colloids Surf. A 265 (2005) 73–80.
[28] D.J. Yates, J. Phys. Chem. 65 (1961) 746.
[29] P.A. Connor, K.D. Dobson, A.J. McQuillan, Langmuir 15 (1999) 2402–2408.
[30] J.T. Carneiro, J.A. Moulijn, G. Mul, Phys. Chem. Chem. Phys. (2010), doi:10.1039/B919886E.
[31] S.H. Szczepankiewicz, A.J. Colussi, M.R. Hoffmann, J. Phys. Chem. B 104 (2000) 9842–9850.
[32] J.T. Carneiro, T.J. Savenije, G. Mul, Phys. Chem. Chem. Phys. 11 (2009) 2708–2714.
[33] T.J. Savenije, M.P. de Haas, J.M. Warman, Int. J. Res. Phys. Chem. Chem. Phys. 212 (1999) 201–206.
[34] J.T. Carneiro, T.J. Savenije, J.A. Moulijn, G. Mul, J. Phys. Chem. C 114 (2010) 327–332.
[35] G. Mul, A. Zwijnenburg, B. van der Linden, M. Makkee, J.A. Moulijn, J. Catal. 201 (2001) 128–137.
[36] A.Y. Nosaka, T. Fujiwara, H. Yagi, H. Akutsu, Y. Nosaka, J. Phys. Chem. B 108 (2004) 9121–9125.
[37] N. Sakai, A. Fujishima, T. Watanabe, K. Hashimoto, J. Phys. Chem. B 107 (2003) 1028–1035.
[38] N. Balazs, K. Mogyorosi, D.F. Sranko, A. Pallagi, T. Alapi, A. Oszko, A. Dombi, P. Sipos, Appl. Catal. B - Environ. 84 (2008) 356–362.